Excerpt from the Proceedings of the 2011 COMSOL Conference in Boston

Transient Pseudo-3D Model of Multi-Beam Laser Thermal Treatment System

Jozef Brcka*
TEL US Holdings, Inc., Technology Development Center
*Corresponding author: 255 Fuller Rd., Albany, NY 12203, jozef.brcka@us.tel.com

Abstract: In this work we modeled scanning laser multi-beam system operating in pulsed regime and used for residual porogen removal from low-k material used in integrated circuit metallization. Pulsed laser beam in motion over semiconductor wafer represents a multi-scale model within large time and space domains. Temperature distribution over wafer depends on many parameters: frequency, duty cycle, beam velocity, path algorithm, polarization-type and incident angle of radiation, microstructure underlying the treated layer and their thermal and optical properties. Expectation from model is to predict transient temperature profiles over the semiconductor wafer that contains structure or film stack composition. Heating power and absorbance have to be accurately formulated by model since thermal and optical properties of each material depend on temperature and wavelength of the laser. Predictive knowledge about temperature profiles is important for DOE validation and process development in low-k dielectric material processing.

Keywords: laser thermal treatment, low-k dielectrics, porogen removal, curring.

1. Introduction

Low-k silicon oxycarbide films (SiOCH hereafter) are very popular for the advanced interconnects because of their chemical stability and compatibility with the traditional ULSI technology. Micro porosity of SiOCH is effectively reducing dielectric constant of low-k film. The SiOCH films are prepared by CVD from gas mixture of source gas, oxidizing gas, porogen and inert gas. Complete removal of porogen residue from SiOCH is important in production of high quality films. Curing process is performed by laser thermal treatment systems (LTTS) which have been used in improving electrical and mechanical properties of low-k dielectric films. The LTTS have wide applications in IC fabrication either for low-k dielectrics or polymer films thermal treatment annealing, polymer curing and resist processing.

Curing of films in production tool[1,2] depends on many factors such as frequency, duty cycle, laser beam velocity, path algorithm, polarization-type and incident angle of radiation, microstructure underlying the treated layer and their thermal and optical properties and micro porosity.

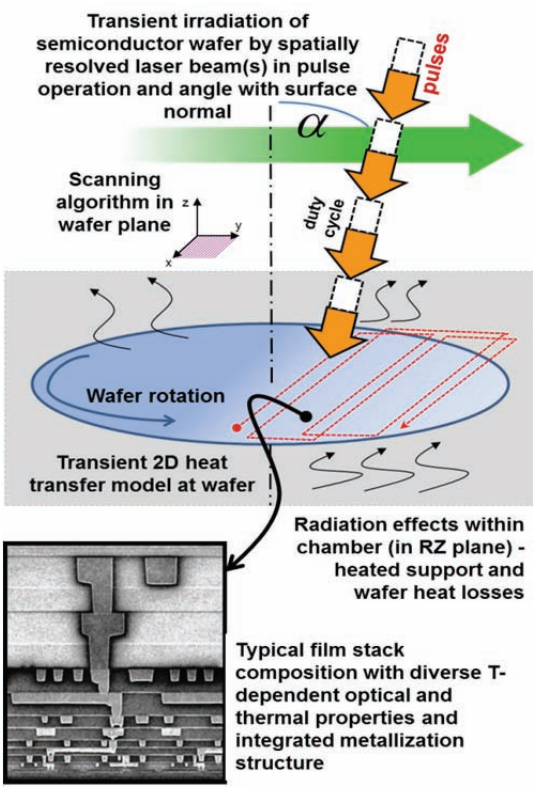

Figure 1: Conceptual scheme of pulsed laser thermal treatment system for semiconductor processing.

From modeling viewpoint process is occurring under multiple time scales and spatial complexity. When heat transfer model is set under "real world" conditions – within characteristic dimensions and process time scales pertinent to today's processing in low-k material treatment, including material complexity, macro *vs.* micro scale variability - the complexity of model will increase substantially. Pure analytical approach is not suitable for explicit

description of all operational conditions. On the other hand the experimental verification is not always feasible.

Numerical modeling of transient heat transfer during semiconductor wafer curing by LTTS can provide accurate information on heating power, absorbance and temperature under complex dependences of thermal and optical properties of involved materials, estimate variability of the process parameters and predict optimal condition. Model description of the composed (multi-) laser beam under pulsing operation and moving according complex path algorithm is given in next section. Analytical approach is described in in Sect. 2.1 and yielding to traveling wave instant radiation source in Sec. 2.2 (macro approach). Materials properties, film stack and structure interpretation by pseudo-domains is given in Sec. 2.3. Next Sec. 2.4 is dealing with formulation of absorbance / reflectance model. Several aspects of complex time sequencing is briefly described in Sec. 2.5. Formulation within COMSOL Multiphysics suite is briefly given in Sect. 3. Sects. 4 and 5 are dealing with the first results and conclusion on this work, respectively.

Expectation from model was to predict transient temperature profiles over the semiconductor wafer that contains metallization structure and/or low-k dielectric film stack composition. Predictive knowledge about temperature profiles is important for DOE validation and process development and helps in interpretation of experimental results.

2. Model description

Model is considering pulsing laser multi-beam LTTS for 300 mm silicon wafers with fast scanning capabilities (linear velocity, *v*, is in range from several cm/s to tens m/s). Transient heat transfer computation is including vertical film stack structure with metallization components (so called vias and wires). Following assumptions are taken into account: (a) laser beam profile has complex spatial shape, *J[x(t),y(t)]*, (this means that also independent laser sub-beams can be formulated in model, here, all sub-beams are synchronized in time); (b) beam is moving over whole wafer area under predefined path algorithm, defined by *x(t)* and *y(t)* functions; (c) laser beam is pulsing at frequency f_R with variable duty cycle ,θ_{ON}, typically 50 %; (d) the pulse overlapping effect occurs during beam motion when beam velocity, v_{beam}, is smaller than product $D_b f_R$ (D_b is beam characteristic dimension); (e) film stack consists of low-k/SiC/(Cu)/Si, and their thermal and optical properties depend on local temperature, *T*; (f) interference effect is neglected in this study; (g) angular dependence of absorption and reflection coefficients is accounted to distinguish between various types of laser polarization; (h) radiation heat/loss transfer from/to surrounding hardware and (i) emissivity at interfaces is neglected.

2.1 Analytical approach

Multi-scale character of the described LTT process was analyzed by several approaches. However, the explicit analytical relationships were too complex and relations had to be implicitly incorporated into numerical FEM model. Let us discuss briefly basic relationships used in model.

In current system the laser beam consists of four sub-beams (indices *"a"* and *"b"* correspond to *x* and *y* coordinates of sub-beam peaks, respectively). Each sub-beam has Gaussian shape. Laser beam is inclined under β angle from vertical axis, thus radiation intensity at surface is given by expression

$$J_{ab}(x,y) = J_{ab}^{0} \cos\beta e^{-\left(x^2\cos^2\beta + y^2\right)/2\sigma^2} \qquad (1)$$

In current case four sub-beams positioned at quadrants in points $\{\pm d;\pm d\}$ will yield a quadruplet profile,

$$J(x,y) = \sum_{a=-1,a\neq 0,b=-1,b\neq 0}^{b=1,a=1} c_{ab} J_{ab}(x,y) \qquad (2)$$

which for $\sigma \sim 4$ mm and $d = 5$ mm will yield beam width approximately D_b~26 mm at e^{-2} level. Parameter c_{ab} is switch parameter and provides an activation (ON/OFF) of particular sub-beam (that means it has value 0 or 1).

Motion and pulsing operation assume that spatial variables depend on time, e.g. *x=x(t)* and *y=y(t)*, and are independent from pulsing function, thus Eq. (1) is rewritten as

$$J_{ab}[x(t),y(t),t] = J_{ab}^{0} \cos\beta e^{-\left(x^2\cos^2\beta + y^2\right)/2\sigma^2} \Gamma(t) \qquad (3)$$

where periodic pulse-function with arbitrary duration of pulse, $\theta_{ON}=f_R T_p$, within period $1/f_R$, is derived in form

$$\Gamma(t) = sign\{[sign[\sin(\pi f_R t)]+1]\times \times\left(sign[-\sin\pi f_R(t-T_p)]+1\right)\}+$$

$$+ sign\{[sign[\sin(\pi f_R t + \pi)]+1]\times$$
$$\times(sign[-\sin\pi f_R((t-T_p)+\pi)]+1)\} \quad (4)$$

Derivation of analytical distribution of the composed laser beam in arbitrary point $\{x;y\}$ on the wafer can be done by integration of Eq. (3) over time however, resultant analytical expression seems to be too complex[3] to be practical for numerical implementation. Considering the overlapping irradiation by subsequent pulses while beam is moving will complicate analytical calculation even more. Reasonable procedure could be averaging over pulse duration however, as we found out, it will deliver approximate solution only, thus loosing analytical accuracy. On the other hand, analytical exercise is useful because it helps to determine important parameters of the laser beam. For example, peak radiation intensity expressed using pulse total power is determined from expression

$$J^{0}_{\substack{a=1\\b=1}} = \frac{P_{total}}{1.908\pi\sigma^2\cos\beta\times erf\left(\sqrt{2}/\cos\beta\right)} \quad (5)$$

Here, *"error"* function can be approximated as

$$erf(x)\approx \mathrm{sgn}(x)\sqrt{1-\exp\left(-x^2\frac{4/\pi+ax^2}{1+ax^2}\right)} \quad (6)$$

where $a = 8(\pi-3)/[3\pi(4-\pi)]$ (7)

2.2 Traveling wave instant radiation source

Following the approach described in section above we derived *"line source"* moving instantly (with velocity *v*) in direction normal to its orientation (*x*-axis) producing wave-like instant radiation source (Fig. 2) moving in *y*-direction

$$\tilde{J}_{quadruplet}(y) = \frac{\sqrt{2\pi}\sigma\times erf\left(\sqrt{2}/\cos\beta\right)}{(d+2\sigma)}\times \quad (8)$$
$$\times J^{0}_{\substack{a=1\\b=1}}\cos^2\beta\left\{e^{-(y-d)^2/2\sigma^2}+e^{-(y+d)^2/2\sigma^2}\right\}$$

This is valid interpretation for fast scans (in range ~ 10 m/s). Note, that Eq. (8) assumes only single pulse irradiation. One can derive effective number of overlapped pulses in form (9) by integration of pulse radiation coming into arbitrary point at wafer surface

$$\left\langle k_{eff}\right\rangle = (1-\theta_{ON})INT\left(\frac{f_R D_b}{v}\right)+\theta_{ON}\frac{f_R D_b}{v} \quad (9)$$

Now, applying product of Eqs. (8) and (9) we obtain *"slowly"* moving *"wave instant radiation source"* in direction normal to wave front (Fig. 2). Details of particular analytical study are out of scope in current paper and will be published separately. It is worth to mention, that incident energy distribution in a semiconductor wafer is subjected to transient heating with radiation due to: (a) radiation absorption and instant source formation, (b) kinetics of heat diffusion, and (c) energy losses – exchange with surroundings and intrinsic consumption of heat in wafer. In dependence on laser operational parameters transient heating may occur in: *Adiabatic regime* - heat distribution depth is much less then thickness of the absorbing layer; *Thermal flux regime* - heat distribution depth is somewhere in between the adsorbing layer depth and wafer thickness; *Heat balance regime* - heat distribution depth is comparable to or greater than the wafer thickness. Conditions in our case are setting model in region between thermal flux and adiabatic regime.

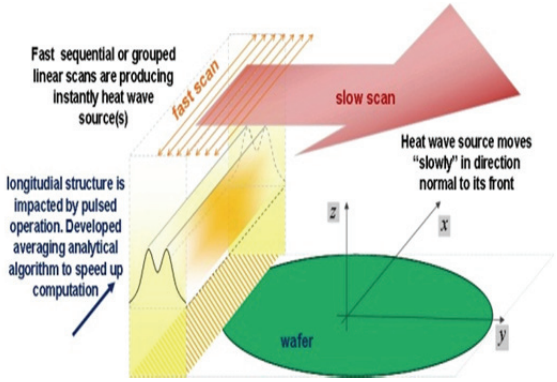

Figure 2: Formation of instant wave radiation source (*"fast line source"* approximation) with *"slow wave"* normal propagation.

2.3 Material properties and structure

Optical and thermal properties of used materials represent extensive part incorporated into actual numerical model and there is not enough space to share all of them in detail within this section. These can be found elsewhere.[4] Present study considered film stack (Fig. 3) that consists of low-k dielectric film (400 nm) on the top of SiC film (35 nm). Further, formally, we are accounting for 10-level metallization below SiC film (for simplicity reasons only single metallization level is used in this contribution). Formation of its micro-structure will be

discussed below. Next domain is representing silicon wafer (thickness ~775 μm). Typically, lower metallization levels are made with SiOCH material, upper levels are made with SiO_2.

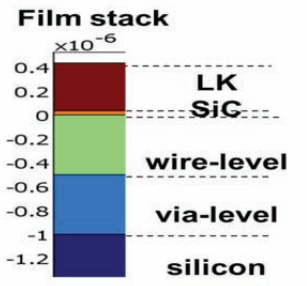

Figure 3: Principal domains assumed in film stack model.

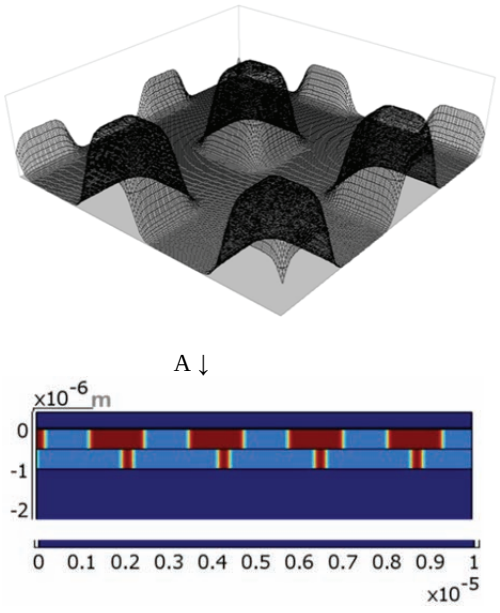

Figure 4: Emulation of via (wire) pseudo-domains within film stack model: a) analytical surface and b) generated by fine meshed numerical model.

Uncured low-k dielectric film *"as deposited"* contains porogen gas. Commercial vendors usually do not disclose detailed information regarding porogen material. It is typically a hydrocarbon having a linear or cyclic structure and expressed by the general chemical formula C_nH_m, wherein n is selected from the group of 4 to 14 while m is selected from group of 4 to 30, and wherein the specific ingredient is selected from the group consisting of α-terpinene, hexane and cyclohexane. In our simulation we will assume that low-k dielectric film deposition was done with porogen ATRP, α-terpinene $Si_\alpha O_{\alpha-1}R_{2\alpha+\beta 2}(OC_nH_{2n+1})$. Actual interpretation of micro porous SiOCH with porogen is under currently ongoing study and its removal will be coupled into numerical solution in next study.

Typical dimensions of metallization are estimated from metal/dielectric area ratio.[5] Assuming typical area ratio for vias is about AR_{via}~1 % and wires, AR_{wire}~30 % we can derive pitch distance in form

$$\bar{d}_{pitch\_via} = (d_{via}/2)\sqrt{\pi/AR_{via}} \quad (10)$$

$$\bar{d}_{pitch\_wire} = \left(d_{wire}/\sqrt{AR_{wire}}\right) \quad (11)$$

Intermediate dielectric (IMD) layer between metallization levels is typically made of SiCN with ~20 nm thickness. Due to single level metallization we neglected presence of such film in our model.

Accurate definition of domains in metallization is unrealistic for FEM model on scale of wafer size. Thus, for lateral distribution of vias and wires we applied periodic rectangular pulse function in spatial coordinates, that is similar to one defined earlier in Sect. 2.1, Eq. (4), that is

$$\begin{aligned}\Gamma_{via}(x) = sign\left(\left[sign\left[\sin\left(\pi x/d_{via\_pitch}\right)\right]+1\right]\times\right.\\ \times\left(sign\left[-\sin\left[\pi(x-d_{via})/d_{via\_pitch}\right]\right]+1\right))+\\ +sign\left(\left[sign\left[\sin\left(\pi x/d_{via\_pitch}+\pi\right)\right]+1\right]\times\right.\\ \left.\times\left(sign\left[-\sin\left[\pi(x-d_{via})/d_{via\_pitch}+\pi\right]\right]+1\right)\right)\end{aligned} \quad (12)$$

In 3D model Eq. (12) is applied also for *y*-coordinate, thus 3D vias are described by product

$$\Gamma_{via}(x,y) = \Gamma_{via}(x)\Gamma_{via}(y) \quad (13)$$

Now we can define also

$$\Gamma_{pitch}(x,y) = 1-\Gamma_{via}(x,y) \quad (14)$$

And metallization density of i^{th} level in 3D model is then

$$\rho^i(x,y) = \Gamma_{via}(x,y)\rho_{cu} + \Gamma_{pitch}(x,y)\rho_{diel} \quad (15)$$

This approach assumes periodically distributed vias and wires (pseudo-domains) and allows us to substantially reduce geometrical setting of metallization domains. It gives substantial flexibility to utilize different properties of dielectric film and Cu-vias in model. Constructed *"metallization structure"* is illustrated on Fig. 4. In similar way we defined thermal conductivity, specific heat, absorption

and reflection coefficients at the i^{th} metallization level, that is

$$k^i(x) = \Gamma^i_{via}(x,y)k_{cu} + \Gamma^i_{pitch}(x,y)k_{diel} \quad (16)$$

$$c^i_p(x) = \Gamma^i_{via}(x,y)c^p_{Cu} + \Gamma^i_{pitch}(x,y)c^p_{diel} \quad (17)$$

$$\alpha^i(x) = \Gamma^i_{via}(x,y)\alpha_{cu} + \Gamma^i_{pitch}(x,y)\alpha_{diel} \quad (18)$$

$$R^i(x) = \Gamma^i_{via}(x,y)R_{cu} + \Gamma^i_{pitch}(x,y)R_{diel} \quad (19)$$

This approach does not require formulation of boundary conditions within metallization structure and allows fast and flexible reset of various vias density at different metallization levels. Typical 10-level metallization of multilevel 65 nm BEOL (back end of line) structure with lightly porous SiOCH film[6] was considered in baseline model. Extensive description of absorption model for such structure and need for frequent flexibility to rework metallization model led us to reduce scheme to single level in pivotal model and include more realistic interpretation of wires and vias (different metal / dielectric area ratios) by splitting into two separate layers (domains). Difference between vias and wires is also in fact that we used cylindrical shape for vias and rectangular shape for wires. Temperature dependent thermal and optical material properties were considered whenever possible and particular expression was derived or approximated for use in discussed model. As source we used several Refs.[4,7,8] and internal experimental resources.

2.4 Absorption model

Absorption/reflection model is assuming following conditions: single forward beam reflections on interfaces only, no return-beam reflection is considered, emissivity at interfaces is neglected, heat loss is considered due to emissivity at top and bottom of wafer, radiation heat transfer from wafer support to wafer was accounted for, and in the case of low-k dielectric material the angular dependence and polarization (*P*, *S* or circular) of absorption, $\alpha_{pol}(\beta)$, and reflection, $R_{pol}(\beta)$, coefficients were used. These coefficients can be approximated by generic function

$$\alpha(\beta) = A_5\cos^5\beta + A_4\cos^4\beta + A_3\cos^3\beta + A_2\cos^2\beta + A_1\cos\beta + A_0 \quad (20)$$

where constants A_k were estimated from experimental data.[8] In multilayer configuration we can formally describe absorption/reflection mechanism by identical formulation which can be applied to each layer in film stack and thus expressed by recurrent formulas. Radiation is substantially attenuated in copper. Absorption in thicker films is also dependent on local value of radiation intensity. Due to diversity of optical properties on microstructure level model should provide accurate description of local radiation source distribution. Assuming $i = 1,2,3,...,N$ is number of layers in model, we can build recurrent formulae for multilayer structure. Initial irradiation is J_0 and we assigned to it a value from Eq. (3) $J[x(t), y(t), t]$. Then transmitted irradiation after passing through the i^{th} layer is given by expression

$$J_i^{trans} = (1-R_i)J_{i-1}^{trans}e^{-\alpha_i h_i/\cos\beta} \quad (21)$$

for $i = 1,2,3,...,N$ and it can be rewritten as

$$J_i^{trans} = (1-R_i)(1-R_{i-1})(1-R_{i-2})... \\ ...(1-R_1)J_0 e^{-(\alpha_i h_i + \alpha_{i-1}h_{i-1} + \alpha_{i-2}h_{i-2} + ... + \alpha_1 h_1)/\cos\beta} \quad (22)$$

for $i = 1,2,3,...,N$. Reflected radiation at the i^{th} interfaces

$$J_i^{refl} = R_i J_{i-1}^{trans} \text{ for } i = 1,2,3,...,N \quad (23)$$

Absorption in the i^{th} layer is derived for single forward pass through the i^{th} layer as

$$J_i^{fwd} = (1-R_i)J_{i-1}^{trans}\left(1 - e^{-\alpha_i h_i/\cos\beta}\right) \quad (24)$$

Distribution of absorbed radiation (heat generation source) per unit volume vs. *z*-coordinate is

$$Q_i^{fwd}(z_{i-fwd}) = (1-R_i)J_{i-1}^{trans}\alpha_i e^{-\alpha_i z_{i-fwd}/\cos\beta} \quad (25)$$

and when reflected from the $(i+1)^{th}$ interface

$$Q_{i,i+1}^{bwd}(z_{i-bwd}) = (1-R_i)R_{i+1} \times \\ \times \alpha_i J_{i-1}^{trans} e^{-\alpha_i(h_i + z_{i-bwd})/\cos\beta} \quad (26)$$

Generalized reflection from the $(i+j)^{th}$ interface will be given by relation

$$Q_{i,i+j}^{bwd}(z_{i-bwd}) = (1-R_i)(1-R_{i+1})(1-R_{i+2})... \\ ....(1-R_{i+j-1})R_{i+j} \times \\ \times \alpha_i J_{i-1}^{trans} e^{-(\alpha_i(h_i + z_{i-bwd}) + 2\alpha_{i+1}h_{i+1} + ... + 2\alpha_{i+j-1}h_{i+j-1})/\cos\beta} \quad (27)$$

where $(j = 2,...,N-i+1)$.

In derivation above we introduced local (implicit) forward z_{i-fwd} and backward z_{i-bwd} coordinate in each i^{th} layer, respectively,

$$z_{i-fwd} = -\left(z + h_1 + h_2 + ... + h_{i-1}\right) - \\ - h_i * floor\left[-\left(z + h_1 + h_2 + ... + h_{i-1}\right)/h_i\right] \quad (28)$$

$$z_{i-bwd} = h_i - z_{i-fwd} \quad (29)$$

Expression for absorbance in the i^{th} layer is further simplified by derivation into form

$$Q_i^{abs}\left(z_{i-fwd}\right) = \left(1-R_i\right)\alpha_i J_{i-1}^{trans} e^{-\alpha_i z_i/\cos\beta} \times \\ \times\left[1+\left(1-R_{i+1}\right)R_{i+2}e^{-\left[\alpha_i\left(h_i+z_{i-bwd}-z_{i-fwd}\right)+2\alpha_{i+1}h_{i+1}\right]/\cos\beta}\right] + \\ + \sum_{j=2}^{N-i+1} Q_{i,i+j}^{bwd}\left(z_{i-bwd}\right) \quad (30)$$

for $\left(j = 2,...,N-i+1\right)$ and $i = 1,2,3,...,N$.

2.5 Timing sequences

Computation of beam propagation should occur on time scale from several μsec to minutes and laser beam path is composed of spatially mixed line/cluster scans. Expressions for internal cycle implicit time (scanning single line) can be described by combination of periodic saw functions and rectangular pulse functions (Fig. 5). For illustration, single scan is done in time $T_{scan} = R_{wafer}/v$ and implicit time within scan is given by

$$t_{scan} = t - T_{scan}\, floor\left(t/T_{scan}\right) \quad (31)$$

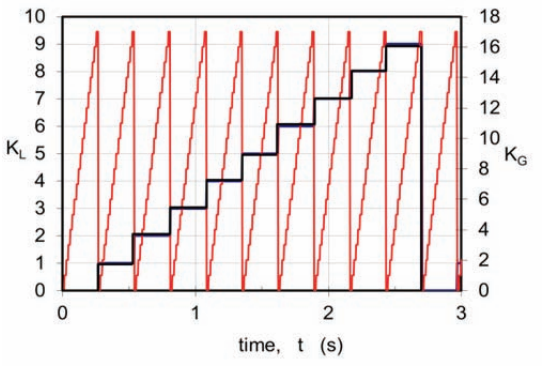

Figure 5: Illustration of multi scale time sequencing implemented for laser beam scan algorithm. K_L stands for number of lines in cluster and K_g is number of clusters.

Velocity of wave propagation in direction normal in respect to line scan will depend on step size, s_g, that is $v_g = s_g/T_{scan}$ where each group contains k_l scans and over wafer radius there is k_g groups. Example of such time sequencing is shown in Fig. 5. There are possible multiple path motions and detail description of time sequencing will depend on actual algorithm. Periodic step-functions are used heavily to complete full process sequence.

3 Use of COMSOL Multiphysics

Actual transient heat transfer model was developed under FEM approach in Multiphysics Comsol v.3.5. Currently, only *General Heat Transfer* module is utilized. Converting *model.mph* into higher version v.4.2 has increased computational speed and it is giving us an opportunity to couple it with *Subsurface Porous Flow* API in future work.

Explicit beam shape, linear motion and pulsed operation initially directed us into explicit analytical formulation of instant radiation source. Later, internal composition of film stack and its structure required to implement implicit formulation of the instant radiation source.

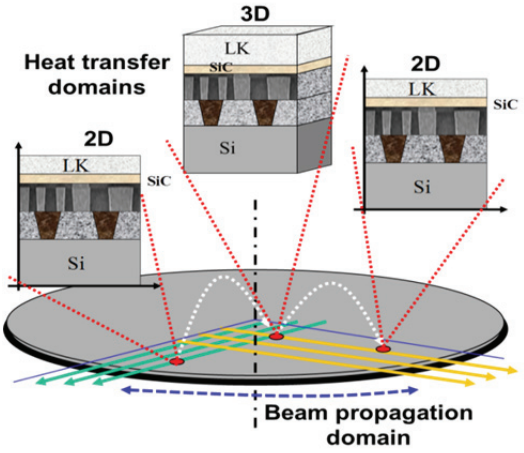

Figure 6: Hybrid transient heat model employing multiple probing volumes (3D) or areas (2D) in preselected observation locations.

Due to computational resources – the first approach allows simulation across planar wafer with limited vertical resolution, the second approach offers output on vertical structure with limited lateral size (only tens microns). We implemented hybrid approach (Fig. 6) that considers laser beam motion within wafer (macro domain) with heat transfer transient model within micro scale domain(s) – represented either by 2D or 3D probing volumes. Such approach requires complex and robust time

stepping. Substantial advantage would be to use a variable-step formulation.

Geometry setting has high aspect ratio either on micro scale (~1:100) or macro scale (~1:400). Meshing scale is from 10 nm to 500 nm. Symmetrical surface boundary conditions (BC) were set at vertical sidewalls of micro-domains. Top and bottom BC are considering radiation losses. Analytical 3D-based model on radiosity from ESC surface is included into boundary conditions at the wafer bottom. Typical time steps were set about 1-25 μs using time dependent solver, PARDISO. Fixed-step solver generates large output files – solution should be saved at preselected times only. We examined change of step size during simulation however, we would like to develop automatic procedure for variable-step solver in future.

4. Results and Discussion

It was apparent immediately from model settings that observation points are exposed by various portions of laser beam radiation profile (Fig. 7). Irradiation will depend on laser beam propagation velocity and motion algorithm, frequency and duty cycle.

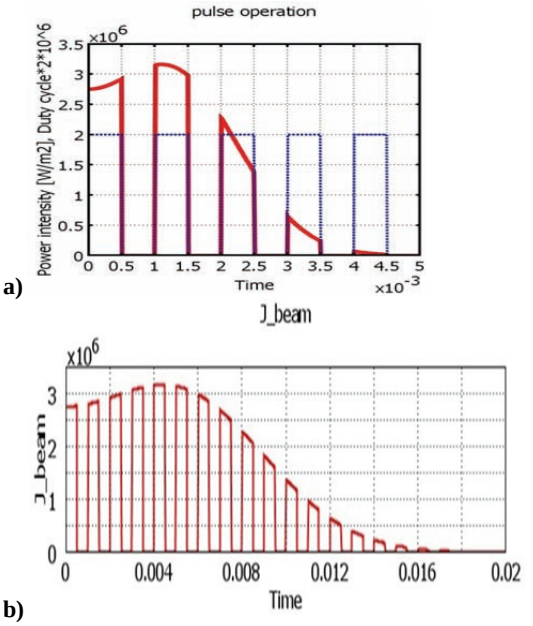

Figure 7: Formation of radiation source, J_{beam} [W/m^2], at 1 kHz (50 % duty cycle) in dependence on laser beam propagation velocity (a) 4 m/s and (b) 1 m/s.

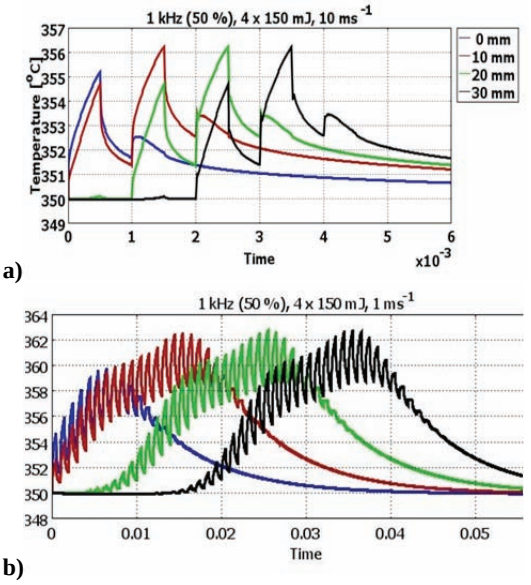

Figure 8: Transient temperature in several observation points distanced 10 mm at propagation velocity (a) 10 m/s and (b) 1 m/s.

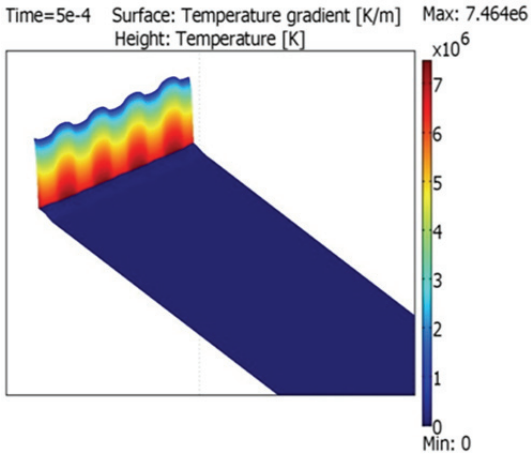

Figure 9: Temperature (height plot) and grad(T) (surface plot) in structure from Fig. 4-b.

Local sub-surface temperature of low-k dielectrics (shown in test structure on Fig. 4-b, readings are taken in point "*A*" in center of 400 nm low-k film and 50 nm below its top surface) increased by ΔT~6 ℃ (Fig. 8-a) comparing to ΔT~12 ℃ (Fig. 8-b) at propagation velocity 10 m/s and 1 m/s, respectively. Metallization structure has impact on local sub-surface temperature (Fig. 9) due to reflection of radiation on metallization structure (assumed 96 % reflection on Cu surface). Temperature gradient

is up to ~ $7x10^6$ K/m nearby an interface with Cu metallization. It is reduced towards the surface of low-k dielectric film.

Transient study of background material impact (Fig. 10-a) on low-k film sub-surface temperature showed there is not significant differentiation in temperature at investigated conditions (Fig. 10-b) though, *grad(T)* is higher in configuration with underlying metal layer (Fig. 10-c).

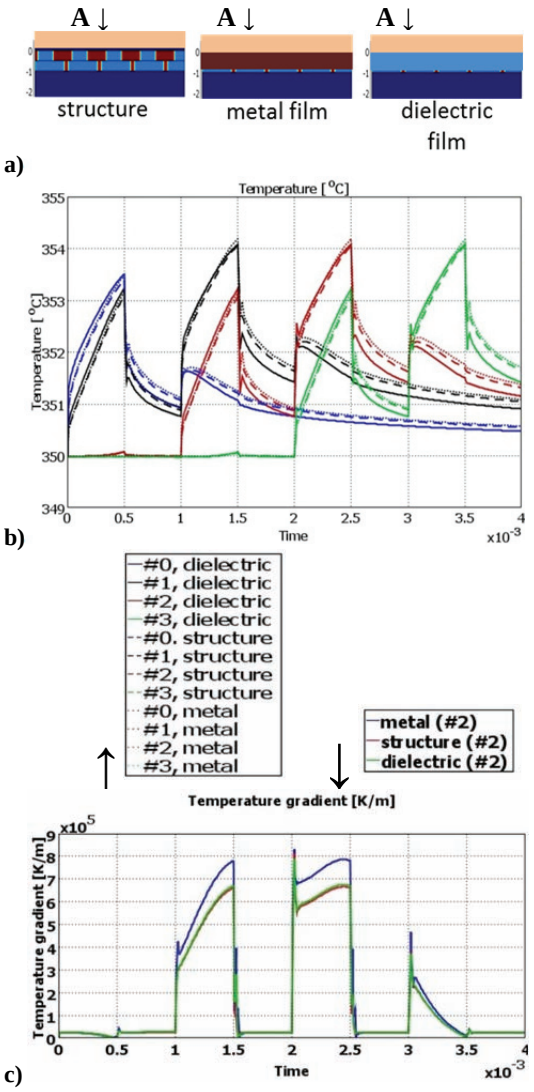

Figure 10: Study on low-k film with underlying material described in diagram (a) shows no significant difference in temperature (b) however, temperature gradient is larger with continuous underlying Cu film (c). Readings are taken in point *"A"* for each probing sub-domain.

Role of *P*, *S* and circular polarization in dependence on the impact angle of laser beam was studied utilizing FEM model. Angular dependence was described in Sect. 2.4 by Eq. (20). Absorbance and reflectance of low-k material have nonlinear dependence on incident angle and polarization type. The highest absorbance and minimum reflectance are observed at Bragg's angle. It was suggested that laser inclination will have impact on subsurface temperature at Bragg's angle. Though, this effect is producing difference in subsurface temperature (blue and green curves in Fig. 11-a), the impact of geometrical aspects is more pronounced (Fig. 11-b) due to strong cosine dependence of radiation intensity. Utilization of polarization effect still make sense however, substantially higher radiation intensity and reduced beam size have to be implemented.

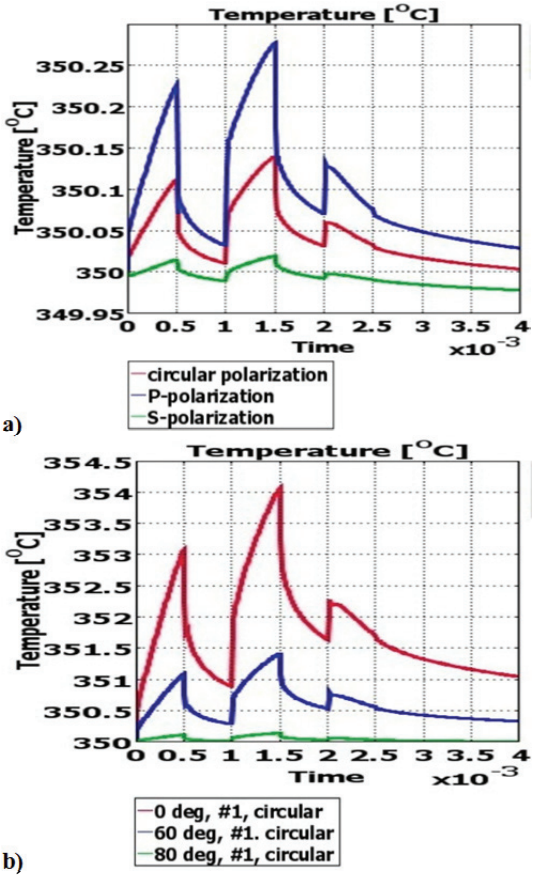

Figure 11: Subsurface temperature for (a) various polarization of laser beam at 80° and angular dependence of temperature for circular polarization (b).

5. Conclusions

In summary, we developed pseudo-3D transient heat transfer model of low-k dielectric films integrated into metallization structure and using an arbitrary speed of CO_2 laser beam with single wavelength in the far IR region for simulation of LTT process for BEOL semiconductor wafers. Modeling allowed us to analyze thermal characteristics during laser treatment. To match real condition and multi scale dimensionality of investigated problem the motion algorithm was designed in expandable way for customized scanning beam path, arbitrary beam profiles and film stack compositions. Further work on this topic will consider detailed experimental and simulation analysis to investigate the variability of the material properties with thermal treatment parameters. Final expectation is to build a flexible model with full functionality to set arbitrary control parameters for process development needs. In future interaction of laser beam with low-k material through activated reactions and mass transport of ATRP porogen through micro porous low-k dielectric material will be considered for inclusion into current FEM model.

6. Acknowledgements

This paper represents modeling contribution to semiconductor tool and process development work that was done by team Dorel Toma, Junjun Liu, Jacques Faguet, Eric Lee, Henry Yue and Yusaku Izawa. Author appreciates discussions with team, technological and application insight on laser thermal treatment processes, tool and experimental observations.

7. References

1. J. Liu, E. Lee and D.I. Toma, Multi-step system and method for curing a dielectric film, *US Pat.* No. 7,622,378 (2009).
2. J. Liu, D.I. Toma and E. Lee, Method for removing a pore-generating material from an uncured low-k dielectric film, *US Pat.* No. 7,977,256 (2011).
3. J. Brcka, *unpublished*, TEH US Holdings, TDC internal reports (2011).
4. V. E. Borisenko, P. J. Hesketh, RTP of semiconductors, Plenum Press, New York (1997).
5. K. Maekawa, *private communication.*
6. V. McGahay, et al, Proceeding of IEEE ITTC 2007, p.196
7. Nilsson, O., H. Mehling, R. Horn, J. Fricke, R. Hofmann, S.G. Muller, R. Eckstein, D. Hofmann, *High Temperatures-High Pressures* 29 (1997), 73-79.
8. J. Liu, *private communication*.